Dynamical detection of a magnetocentrifugal wind driven by a 20 M⊙ YSO

L. J. Greenhill[1], C. Goddi[2], C. J. Chandler[3], E. M. L. Humphreys[2], and L. D. Matthews[4]

[1]Harvard-Smithsonian CfA, 60 Garden St, Cambridge, MA, USA
email: greenhill@cfa.harvard.edu

[2]ESO, Karl-Schwarzschild-Strasse 2, 85748 Garching, Germany
email: cgoddi@eso.org, ehumphre@eso.org

[3]NRAO, PO Box O, Socorro, NM, USA
email: cchandle@nrao.edu

[4]MIT Haystack Observatory, Off Route 40, Westford, MA, USA
email: lmatthew@haystack.mit.edu

Abstract. We have tracked the proper motions of ground-state λ7mm SiO maser emission excited by radio Source I in the Orion BN/KL region. Based on dynamical arguments, Source I is believed to be a hard 20 M⊙ binary. The SiO masers trace a linear bipolar outflow (NE-SW) 100 to 1000 AU from the binary. The median 3D velocity is 18 km s^{-1}. An overlying distribution of 1.3 cm H_2O masers betrays similar characteristics. The outflow is aligned with the rotation axis of an edge-on disk and wide angle flow known inside 100 AU. Gas dynamics and emission morphology traced by masers around Source I provide dynamical evidence of a magnetocentrifugal disk-wind around this massive YSO, notably a measured gradient in line-of-sight velocity perpendicular to the flow axis, in the same direction as the disk rotation and with comparable speed. The linearity of the flow, despite the high proper motion of Source I and the proximity of dense gas associated with the Orion Hot Core, is also more readily explained for a magnetized flow. The extended arcs of ground-state maser emission bracketing Source I are a striking feature, in particular since dust formation occurs at smaller radii. We propose that the arcs mark two C-type shocks at the transition radius to super-Alfvénic flow.

Keywords. ISM: individual (Orion KL) — ISM: jets and outflows — ISM: Kinematics and dynamics — ISM: molecules — masers — stars: formation

1. Orion BN/KL

The predominant outflow in Orion BN/KL ($\sim$420 pc distant) is an uncollimated expansion of up to 300 km s^{-1}, traced by shocked fingers of H_2 and by high-velocity CO. It is not directly tied to any of the known YSOs. Rather, the apparent origin is proximate (in time and position) with the closest approach of three YSOs (radio Source I, infrared source n, and the BN object) inferred from their diverging proper motions (Gómez *et al.* 2008, Goddi *et al.* 2011a, Bally *et al.* 2011). With regard to this inferred dynamical history, BN/KL may indeed be unusual, but elements are familiar, specifically a disk-outflow model of Source I . The gas structure and dynamics have been resolved in studies of SiO and H_2O masers (Goddi *et al.* 2009, and references therein). In these studies, the position-velocity structure of the SiO masers, resolved with very long baseline interferometry (VLBI), has been shown to outline a disk and bipolar wide-angle outflow at radii of 10-100 AU (Greenhill *et al.* 2004, Matthews *et al.* 2010, Kim *et al.* 2008), where proper motions clearly separate outflow and rotating disk components (Matthews *et al.* 2010).

Table 1. Observing Log

| Date (yymmdd)	Tracer	Array	Beam (mas) (°)		RMS[a] (mJy)
1999.08.28	SiO v=0, 1	A+	61×43 @ $+44°$		10-40
2002.03.31	SiO v=0, 1	A+	55×45 @ $-31°$		6-20
2006.04.15	SiO v=0, 1	A+	53×39 @ $-3.8°$		2.5-8.5
2009.01.12	SiO v=0, 1	A	53×43 @ $+3.6°$		3-20
2001.01.23	H_2O $6_{16} - 5_{23}$	A+	113×48 @ $+30°$		> 6

[a] For a $1.3 \, \mathrm{km \, s^{-1}}$ channel. Images were dynamic range limited.

We describe the angular distributions and evolution of ground-state $\lambda 7 \, \mathrm{mm}$ SiO and $\lambda 1.3 \, \mathrm{cm}$ H_2O maser emission at radii of 100 to 1000 AU around Source I . The data reported here densely sample the outflow. A self-consistent picture of a high-mass YSO emerges that reinforces the disk-outflow model for 10-100 AU, introduces the prospect of a magnetic field that is dynamically important at radii up to a few $\times 100 \, \mathrm{AU}$, and suggests an explanation for excitation of the ground-state SiO and the H_2O masers.

2. Observations and Data Reduction

We observed two transitions of SiO and one of H_2O toward Source I with the NRAO VLA at multiple epochs over 9 years (Table 1).

SiO– At each epoch, we correlated two simultaneous, single-polarization basebands, one tuned to the $v = 0$ transition and the other to the much stronger $v = 1$ transition. We used a $6.25 \, \mathrm{MHz}$ bandwidth ($-13.7 < \mathrm{V_{lsr}} < 29.4 \, \mathrm{km \, s^{-1}}$) and $97.656 \, \mathrm{kHz}$ ($0.65 \, \mathrm{km \, s^{-1}}$) channel spacing. We selected a strong $v = 1$ Doppler component as a reference to self-calibrate antenna gain and tropospheric fluctuations on 10-second time scales. Scans of
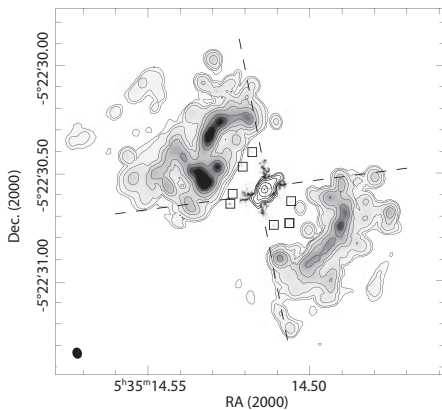
Figure 1. Nested tracers around Source I at $\lambda 7 \, \mathrm{mm}$. Velocity-integrated flux from the $v = 0$ $J = 1 \to 0$ transition of SiO (grayscale with contours) brackets continuum emission from Source I - contours at center (Goddi *et al.* 2011a). Extending away from the continuum source in four arms is $v = 1$ and $v = 2$ SiO maser emission, mapped with VLBI (Matthews *et al.* 2010), chiefly at radii $< 50 \, \mathrm{AU}$; isolated clumps of emission are outlined for clarity (boxes). The arms delimit the edges of a wide angle outflow directed NE-SW (dashed lines).
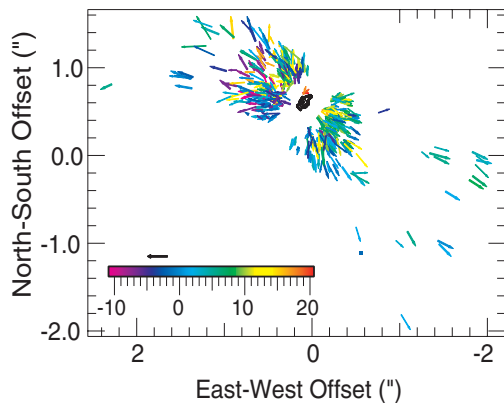
Figure 2. Outflow at radii of 10-1000 AU from Source I, including outward proper motions for SiO $v = 0$ emission clumps from 1999 to 2009 (bars). Contours show $\lambda 7 \, \mathrm{mm}$ continuum emission that marks the relative location of Source I as in Figure 1. Colors indicate LSR radial velocity in $\mathrm{km \, s^{-1}}$ (color bar); the systemic velocity is $5 \, \mathrm{km \, s^{-1}}$. The horizontal black arrow indicates a proper motion of $30 \, \mathrm{km \, s^{-1}}$.

J0541–056 enabled calibration of slowly varying phase offsets between the signal paths for the two observing bands, which enabled us to transfer the antenna and tropospheric calibration to the band containing the (weaker) $v = 0$ line. Absolute and relative astrometry of the maser emission, using close by BN and J0541–0541 as references, was thermal noise limited (Table 1). Registration with respect to Source I is accurate to ~10 mas.

We tracked proper motions for 447 $v = 0$ spots for between 2 and 4 epochs ($> 5\sigma$). Lifetimes were in excess of several years, much stronger than for $v = 1$ and 2 features. To estimate proper motions for each channel map, we fit each spot with a two-dimensional elliptical Gaussian. Images of $v = 0$ emission were noise-limited, and the relative position errors were given by beamwidth divided by $2\times$ SNR per channel, or a few mas for moderately bright emission. Cross-referencing of maser spots among different epochs could be done by eye because the structure of the emission in each velocity channel persisted. Proper motions were calculated using an error-weighted linear least-squares fit to fitted positions. To correct for the motion of the reference $v = 1$ Doppler component, we computed proper motions relative to the strong $v = 0$ feature at $+2.7$ km s^{-1} (imparting to it an apparent zero motion) and then subtracted the mean motion of all those measured ($\dot{\alpha} = 6.11 \pm 0.02$ km s^{-1} and $\dot{\delta} = 23.26 \pm 0.04$ km s^{-1}).

H$_2$O– We observed H$_2$O maser emission between $V_{lsr} = -138$ and 137 km s^{-1} and report here on emission detected in the so-called H$_2$O Shell (Genzel *et al.* 1981) that is associated with Source I (Table 1). We divided the source spectrum into overlapping 1.56 MHz bands and observed these in pairs with 0.16 km s^{-1} channel spacing after Hanning smoothing. One band within each pair was tuned to include the line emission peak near -4.5 km s^{-1}. We used the emission at -3.86 km s^{-1} (1700 Jy) to obtain self-calibration solutions every 10 seconds. Scans of J0541–056 every 45 minutes enabled calibration of instrumental phase offsets between bands. Registration of emission in the different bands is accurate to < 2 mas. Absolute astrometry was derived from calibration against J0541–0541. The same techniques were used to predict the position of J0605–085, achieving an absolute position uncertainty of 2 mas. From detection of BN in continuum and pseudo-continuum images toward Source I, we
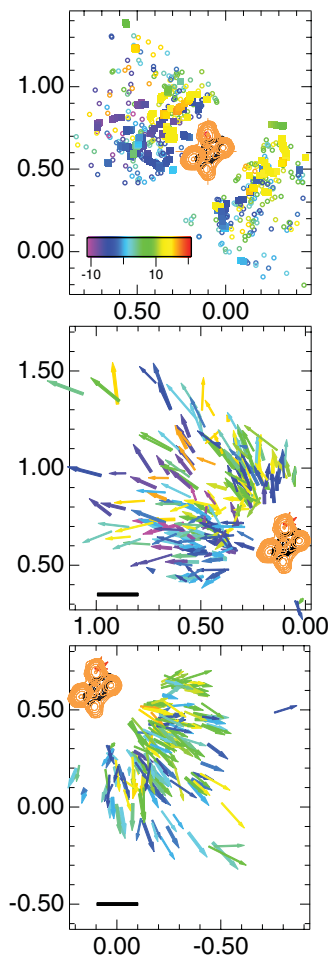
Figure 3. (*top*) SiO $v = 0$ and H$_2$O masers (open circles and squares, respectively), velocity-integrated SiO $v = 1$ masers as mapped with the VLA (orange contours), and the Source I $\lambda 7$ mm continuum (black contours; see Figure 1). (*middle*) Proper motions for SiO emission clumps, 1999 to 2009, expanded to show proper motions in the lobe northeast of Source I . (*bottom*) Expanded view to the southwest. The horizontal black bar corresponds to a proper motion of 40 km s^{-1} in one year.

obtained for BN a J2000 position of $05^h 35^m 14\overset{s}{.}1131$, $-05°22'22''\!.794$ with 3 mas uncertainty (epoch 2001.06). This lies $\sim 1\sigma$ from the trend line at 22 GHz of Rodriguez *et al.* (2005) for epoch 2001.06 (offset 13 and 2 mas in right ascension and declination, respectively). We also detected continuum emission of Source I at 6σ, lying $+5''\!.950$ and $-7''\!.737$, $\pm 0''\!.007$ with respect to BN. The difference from the measurement of Rodriguez *et al.* (2005) is $(+2, -6)$ mas or $< 1\sigma$ (cf. Goddi *et al.* 2011a).

3. Discussion

Morphology & Dynamics– The most intense $v = 0$ SiO maser emission occupies two arcs bracketing Source I, at a radius of ~ 100 AU. This is just outside the maximum radius at which isolated $v = 1$ masers are observed (Figure 1). The arcs subtend about the same opening angle as the nearly radial arms at smaller radii along which $v = 1$ and $v = 2$ emission features move outward. This is believed to trace the edges of a bipolar outflow orthogonal to the edge-on disk whose rotation the vibrationally excited emission also traces (Matthews *et al.* 2010).

The angular and velocity structure of the $v = 0$ emission is suggestive of outflow in the plane of the sky; there is no offset in the mean velocities of the two lobes, at the $O(1)$ km s^{-1} level. The median proper motion for maser spots tracked for >2 epochs is 18 km s^{-1}, and the range of 3D velocities in the local frame ($V_{LSR} = 5$ km s^{-1}) is 4 to 36 km s^{-1}. The H_2O emission displays a similar range of line-of-sight velocity. A 20 km s^{-1} expansion in the angular extent of the distribution over ~ 8 years (Greenhill *et al.* 1998) is consistent with the median SiO maser proper motion. The mean position angle measured from the emission locus and separately from the proper motions is $56°$.

The linearity of the outflow is notable because (i) Source I lies at the edge of the dense gas associated with the Orion Hot Core (Goddi *et al.* 2011b), (ii) the 18 km s^{-1} outflow is comparable to the 12 km s^{-1} proper motion of the YSO toward the densest portion of the Hot Core, (iii) SiO maser dynamics inside $O(1000)$ AU are indicative of a ~ 500 yr dynamical time for the outflow, and (iv) the crossing time for Source I from the point at which the YSO underwent dynamical interaction with BN (separation 50 AU on the sky) is also ~ 500 yr (i.e., the flow is contemporaneous with the interaction with BN).

For hydrodynamic flow, there being no sweeping back suggests that the momentum flux exceeds that of the ambient medium into which Source I is moving. Ground-state SiO maser emission requires densities of 10^6-10^7 cm^{-3} for collisional pumping (e.g., Goddi *et al.* 2009). Given the comparable velocities (12 vs 18 km s^{-1}), the density of ambient material must be $\ll 10^6$ cm^{-3} (still less if the maser medium reflects enhancement over the mean flow density, as by shocks). However, ambient gas densities in the vicinity of the Hot Core are large, $O(10^6)$ cm^{-3} (e.g., Goddi *et al.* 2011b), and as a result some deflection may be anticipated. Alternatively, there could be a fast flow due to stellar winds ($O(100)$ km s^{-1} for a $10_\odot$ B-star) that fragments and infiltrates the ambient material, generating a trail of maser emission, but limb brightening along leading edges and asymmetry in response to density gradients (which is not seen) would be anticipated.

Magnetocentrifugal Wind– The alternate possibility of a magnetohydrodynamic disk wind is raised by a discernible rotation signature about the major axis of the flow in each lobe. Toward the SE-facing edge, there is a greater preponderance of blueshifted emission; redshifted emission lies preferentially toward the NW. There is considerable scatter about this trend (e.g., there is still relatively blue shifted emission toward the NW face), but it is parallel and only somewhat smaller (15-20 km s^{-1} vs 20-30 km s^{-1}) than the offset seen plainly among vibrationally excited SiO masers at radii of tens of AU and from which rotation is inferred (Matthews *et al.* 2010).

The data presented here are suggestive of these dynamics being communicated from scales of O(10) AU to at least O(100) AU. The most natural mechanism would be action by magnetic field lines threading the flow. This addition also raises the energy density in the flow and more readily enables linear flow in a dense medium. We note that re-assessment of data for the vibrationally excited SiO masers provides some confirming evidence. Matthews *et al.* (2010) conservatively interpreted the maser data in the context of Keplerian motion and the dominant action of gravity (cf. Kim *et al.* 2008), inferring a dynamical mass of $\sim 8\,M_\odot$. However, the value is inconsistent with the more direct estimate of $20\,M_\odot$ obtained by Goddi *et al.* (2011a) under the assumption that BN and Source I are in recoil. Hence, reproducing the SiO dynamics observed with VLBI requires invocation of non-gravitational forces as well.

Super Alfvénic Flow– Why does intense ground-state SiO and H_2O maser emission arise suddenly at 100AU? Why are SiO and H_2O masers apparently intermixed when the densities required for emission differ by (conservatively) an order of magnitude? For a YSO luminosity on the order of $2\times10^4\,L_\odot$ (i.e., $2\times10\,M_\odot$), the sublimation radius of dust will be $\ll 100\,$AU, and since maser emission requires a high gas phase abundance, its appearance so far out and over a significant interval of the flow are significant.

We propose that the arcs of maser emission at $\sim 100\,$AU radius indicate the onset of strong shocks in dusty outflowing material. Hydromagnetic C-type shocks as slow as 10-$20\,\mathrm{km\,s^{-1}}$ (comparable to the flow speed) are capable of sputtering grains (Schilke *et al.* 1997), a process that would raise gas phase abundance of SiO and H_2O. Formation of two continuous shock structures subtending broad ranges of polar angle and narrow ranges in radius indicates a systematic change in physical conditions. Transition to a super Alfvénic flow and consequent shock formation may trigger the observed (re)appearance of maser emission in the outflow at $\sim 100\,$AU. Conditions conducive to shocks will arise if the Alfvén velocity declines with radius and crosses the outflow velocity, which does not vary considerably with radius. Where density falls quadratically, this may occur if the field declines at least linearly (not unlikely). One observational prediction of this proposal is that the inner edge of maser emission will not expand on the sky with time.

Maintenance of gas phase abundance well downstream, as indicated by preponderance of maser emission there, suggests that high gas phase abundance and pump excitation persist. In view of flow speed in excess of sound and Alfvén speeds, continued shocking may be expected, although long cooling timescales may also be responsible. In this region, fading of the velocity gradient along the flow minor axis and concomitant redirection of proper motions to be more downstream suggests increasing decoupling of the neutral gas from the field, as anticipated in MHD disk wind models.

References

Bally, J., Cunningham, N. J., Moeckel, N., *et al.* 2011, *ApJ*, 727, 113
Genzel, R., Reid, M. J., Moran, J. M., & Downes, D. 1981, *ApJ*, 244, 884
Goddi, C., Greenhill, L. J., Chandler, C. J., *et al.* 2009, *ApJ*, 698, 1165
Goddi, C., Greenhill, L. J., Humphreys, E. M. L., *et al.* 2011b, *ApJ*, 739, L13
Goddi, C., Humphreys, E. M. L., Greenhill, L. J., *et al.* 2011a, *ApJ*, 728, 15
Gómez, L., Rodríguez, L. F., Loinard, L., *et al.* 2008, *ApJ*, 685, 333
Greenhill, L. J., Gwinn, C. R., Schwartz, C., *et al.* 1998, *Nature*, 396, 650
Greenhill, L. J., Gezari, D. Y., Danchi, W. C., *et al.* 2004, *ApJ*, 605, L57
Kim, M. K., *et al.* 2008, *PASJ*, 60, 991
Matthews, L. D., Greenhill, L. J., Goddi, C., *et al.* 2010, *ApJ*, 708, 80
Rodríguez, L. F., Poveda, A., Lizano, S., & Allen, C. 2005, *ApJL*, 627, L65
Schilke, P., Walmsley, C. M., Pineau des Forets, G., & Flower, D. R. 1997, *A&A*, 321, 293